Letters

Design and Analysis of a Wireless Ultrasonic Motor Drive System

Yang Xiao, *Member, IEEE*, Yong Yang, *Senior Member, IEEE*, Chunhua Liu, *Senior Member, IEEE*, and Jose Rodriguez, *Life Fellow, IEEE*

***Abstract*—In this letter, a novel wireless motor system, namely, the wireless ultrasonic motor (WUM) system, is proposed and analyzed. A unique wireless drive topology is designed to solve the problems of the existing wireless drives, such as complex controller and converter at both the transmitting and receiving sides, regular maintenance, and output ripple resulted from motor type and control scheme. The key is to combine the merits of the wireless power transfer and ultrasonic motor to wirelessly energize the ultrasonic motor with high-frequency voltage directly. Meanwhile, a matching inductor is designed for the proposed wireless drive to improve power quality and to filter harmonic voltages at the motor side. Furthermore, laminated coil structure is optimized with electromagnetic decoupled ability and less ferrite core. Two-mode motor control method is designed to extend the speed range of the proposed WUM drive. Finally, operating principles and experimental results are provided to verify the feasibility and correctness of the proposed WUM drive system.**

***Index Terms*—Ultrasonic motor, wireless motor drive, wireless power transfer.**

I. Introduction

DUE to the distinct advantages of convenience, safety, and electrical isolation, wireless power transfer has achieved great development in recent decades [1]. It has been increasingly investigated and applied in various applications, for example, wireless charging [2], wireless heating [3], wireless lighting [4], and wireless drive [5], [6], [7]. Particularly, the concept of the wireless drive has been conceived, which can eliminate the metallic connection and wire abrasion to facilitate the motor operation in a harsh and watery environment.

However, it suffers from adopting controllers and converters in both the transmitting and receiving sides, which will undoubtedly increase the system complexity and decrease the reliability [8], [9]. Thus, it is highly preferable to develop the wireless drive system without employing any converters and controllers in the receiver side in compact situation if bidirectional power flow is not needed.

To solve this problem, a wireless dc motor drive system simplified the converter design by replacing by two MOSFETs at the receiving side [10]. However, the carbon brushes and commutator of the wireless dc motor need regular maintenance, which is inconvenient in harsh environments. In order to avoid the use of carbon brushes and commutator, the wireless switched reluctance motor is recently proposed in [11] and [12]. Three different resonant frequencies are usually needed to separately activate three-phase of motor windings. It is usually realized by capacitor matrix or two *LCC* compensation circuits, which is bulky and heavy. Furthermore, the torque ripple of the wireless switched reluctance motor makes it not suitable for precise control systems. Wang et al. [13] proposed a wireless shaded-pole induction motor drive system. Similarly, the multifrequency transmission, which needs bulky compensator, is necessary to ensure normal operation. Meanwhile, numerous MOSFETs and self-driving circuits at the receiving sides are adopted to equalize the output phase currents, which is contrary to the original intention of the wireless drive.

A new wireless drive structure named wireless ultrasonic motor drive system (WUM) is proposed in this letter for precise motion platform in vacuum chamber or valve control in isolated environment. The novelty is summarized as follows: 1) the proposed wireless drive system guarantees that no controller or active device exists at the transmitting side; 2) the proposed system can avoid the regular maintenance and output ripple resulted from other wireless drives; 3) the proposed wireless drive combines the merits of the ultrasonic motor, including small volume, low-speed high torque output, high control accuracy, fast response, and off-power self-locking ability; and 4) the proposed two-mode speed control can extend the speed range of the wireless drive.

II. Design and Operating Principles

A. System Topology Design

Fig. 1 shows the circuit configuration of the proposed wireless motor drive system. As demonstrated, it contains the H-bridge inverter, two *LC* compensating circuits at the transmitting side,

Manuscript received 17 May 2023; revised 13 June 2023; accepted 24 June 2023. Date of publication 3 July 2023; date of current version 1 September 2023. This work was supported in part by the Nature Science Youth Foundation of Jiangsu Province under Grant BK20220499, and in part by the Chinese Postdoctoral Science Foundation under Grant 2022M711394. *(Corresponding author: Yong Yang.)*

Yang Xiao and Yong Yang are with the School of Rail Transportation, Soochow University, Suzhou 215006, China (e-mail: yangxiao@suda.edu.cn; yangy1981@suda.edu.cn).

Chunhua Liu is with the School of Energy and Environment, City University of Hong Kong, Hong Kong (e-mail: chualiu@eee.hku.hk).

Jose Rodriguez is with the Faculty of Engineering, Universidad San Sebastian, Concepción 4030000, Chile (e-mail: jose.rodriguezp@uss.cl).

Color versions of one or more figures in this article are available at https://doi.org/10.1109/TPEL.2023.3291749.

Digital Object Identifier 10.1109/TPEL.2023.3291749

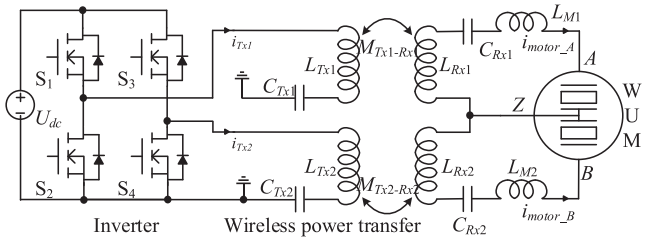

Fig. 1. Circuit diagram of proposed wireless ultrasonic motor drive system.

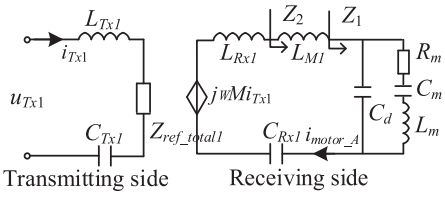

Fig. 2. Equivalent circuit of one-phase stator model.

two *LC* compensating circuits at the receiving side, and the ultrasonic motor. The power switch S_1 and S_2 generate the high-frequency voltage for the first channel wireless power transmission, while the power switch S_3 and S_4 generate the high-frequency voltage for the second channel wireless power transmission. The two wireless power transmission channels are independent in frequency, duty cycle, and phase position to drive the two-phase of the WUM.

B. System Analysis

The C_{Tx1}, C_{Tx2}, C_{Rx1}, and C_{Rx2} are capacitance of the compensation capacitors, while the $L_{Tx1}, L_{Tx2}, L_{Rx1}$, and L_{Rx2} are the inductance of the transmitting coils. They follow the mathematical relation

$$\begin{aligned} C_{Tx1} &= \left(\omega_r^2 L_{Tx1}\right)^{-1}, C_{Rx1} = \left(\omega_r^2 L_{Rx1}\right)^{-1} \\ C_{Tx2} &= \left(\omega_r^2 L_{Tx2}\right)^{-1}, C_{Rx2} = \left(\omega_r^2 L_{Rx2}\right)^{-1} \end{aligned} \tag{1}$$

where ω_r is the operating angular frequency and it can be calculated by $2\pi f_{\mathrm{r}}$, and f_r is the resonant frequency.

The equivalent electrical model of one phase of the WUM can be expressed as [14], [15], [16]

$$Z_1 = \frac{1}{j\omega C_d} \parallel \left(R_m + j\omega L_m + \frac{1}{j\omega C_m}\right) \tag{2}$$

where C_d is the equivalent parallel capacitor, R_m is the equivalent series resistor, C_m equivalent series capacitor, L_m is the equivalent series inductor, and ω is the operating frequency. The series and parallel resonant frequency exist in the equivalent electrical model of the WUM, they follow the relation

$$\omega_s^2 L_m C_m = 1, \omega_p^2 L_m C_d C_m = C_d + C_m. \tag{3}$$

When the ultrasonic motor is operating near the resonant frequency, the motor it often treated as a capacitance load. Thus, a matching circuit is often designed to improve operating characteristics [8]. The matching component has two functions. First, it can filter high-frequency voltage, which is regarded as a low-pass filter. So the operating characteristic can be improved compared with no matching component. Second, the matching component can change the equivalent resonant frequency to reduce the reactive power and current stress. It needs to mention that many circuits can be used as matching circuits, like T-type, *LC* type, *LLC*, and *LCL* types. The compensation effects may differ, but an inductor is chosen in this letter to simplify the receiving-side circuits, and the equivalent circuit is shown in Fig. 2.

The impendence of receiving side with matching circuits

$$Z_{Rx1} = j\omega L_{R1} + \frac{1}{j\omega C_{R1}} + j\omega L_{M1} + Z_1. \tag{4}$$

The reflecting impendence of the WUM

$$Z_{\mathrm{ref\_total1}} = \frac{(\omega M)^2}{Z_{Rx1}}. \tag{5}$$

Using Kirchhoff's law, the following equations are derived:

$$\begin{cases} (j\omega L_{Tx1} + \frac{1}{j\omega C_{Tx1}} + Z_{\mathrm{ref\_total1}}) i_{Tx1} = U_{Tx1} \\ j\omega M i_{Tx1} = i_{\mathrm{motor\_}A} Z_{Rx1} \end{cases}. \tag{6}$$

Assume the wireless power transfer circuit operates at the ideal resonant frequency, then the gain of the receiving side with matching inductor is

$$\begin{aligned} G_v = &\frac{R(R - CL_{M1}R\omega^2)}{L_{M1}^2\omega^2 + (R - CL_{M1}R\omega^2)^2} \\ &- \frac{jL_{M1}R\omega}{L_{M1}^2\omega^2 + (R - CL_{M1}R\omega^2)^2} \end{aligned} \tag{7}$$

$$\begin{aligned} R = R_m + \frac{\omega^2 L'^2_m}{R_m},\ C = C_d - \frac{L'_m}{R_m^2 + \omega^2 L'^2_m}, \\ L'_m = L_m - \frac{1}{\omega^2 C_m}. \end{aligned} \tag{8}$$

To increase gain and decrease reactive power, the imaginary part of gain should be as small as possible. Thus, the L_{M1} should be

$$L_{M1} = \frac{R^2 C}{1 + R^2 C^2 \omega^2}. \tag{9}$$

Substituting (8) into (9), the final matching inductor can be derived:

$$L_{M1} = \frac{C_d L_m^2 \omega^2 + C_d R_m^2 - L_m}{C_d^2 L_m^2 \omega^4 + C_d^2 R_m^2 \omega^2 - 2C_d L_m \omega^2 + 1}. \tag{10}$$

Assume the wireless power transfer circuit and the ultrasonic motor both operate at the ideal resonant frequency, the transmitting side current i_{Tx1} and voltage U_{Tx1} should be in the same phase, which means the total reflecting impendence with matching inductor is resistive.

The phase delay between the transmitting-side and receiving-side voltages is not considered. This is because according to the characteristics of the ultrasonic motor, only the phase difference between the two-phase voltages u_{AZ} and u_{BZ} will influence the motor statues rather than phase delay between the transmitting-side and receiving-side voltages.

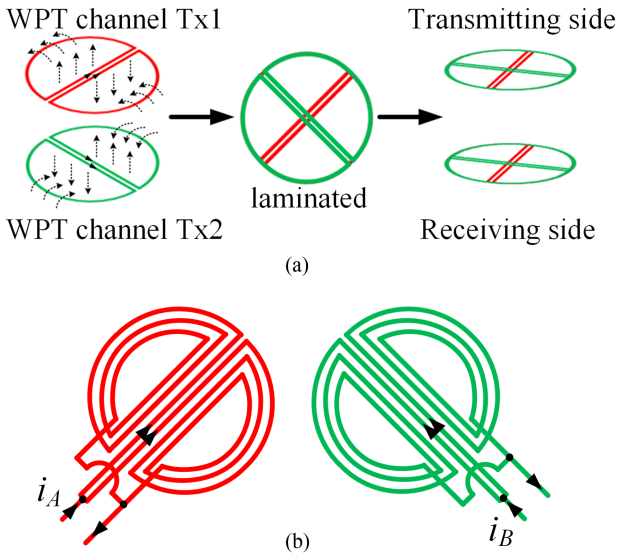

Fig. 3. Laminated four-D coils design. (a) Configuration of transmitting and receiving coils. (b) Electric connection of coils.

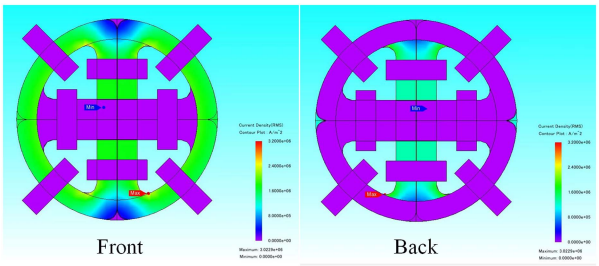

Fig. 4. FEM simulation of laminated four-D coils.

C. Coupling Structure

The transmitting coils and receiving coils are avoided to adopt discrete structure to decrease coil size. Thus, a laminated four-D structure [17] is used here to improve power density, as shown in Fig. 3. The transmitting and receiving coils are composed of the four D-type coils. The first and the second two D-type coils are laminated together and their position is perpendicular to each other. The receiving coils are formed and connected in the same way as the transmitting coils.

The coupling structure can transfer wireless energy to the targeted coils, while tremendously avoiding electromagnetic coupling with nontargeted coils. For example, the transmitting coil T_{X1} is designed to transfer energy to R_{X1}, while no energy is expected to transfer to T_{X2} and R_{X2}. Meanwhile, T_{X2} is designed to transfer energy only to R_{X2}, rather than T_{X1} and R_{X1}.

Compared with the laminated four-D structure in [17], the ferrite core of the coupling structure is redesigned and optimized. The most remarkable difference is that less ferrite core is used here while achieving similar coupling effect. Fig. 4 shows the finite-element simulation of the redesigned coupling structure. It can be seen from the current density of the coils that only targeted coils can receive wireless energy from the corresponding transmitting coils.

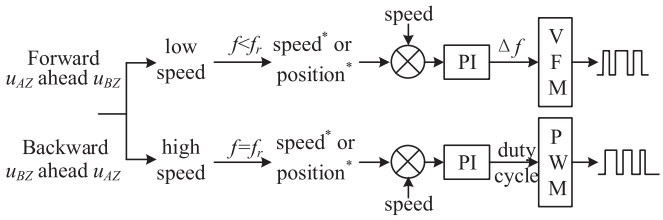

Fig. 5. Wireless ultrasonic motor control block.

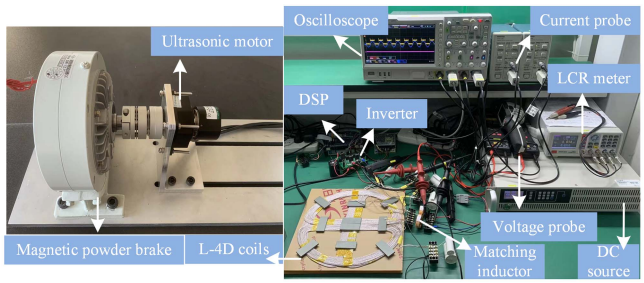

Fig. 6. Experimental prototype.

TABLE I
KEY EXPERIMENTAL PARAMETERS

Parameter	Value	Parameter	Value
Input voltage	10 Vdc	Matching inductance	2 mH
Inductance of T_{X1}	55.22 μH	Inductance of R_{X1}	55.23 μH
Capacitance of T_{X1}	286 nF	Capacitance of R_{X1}	286 nF
Inductance of T_{X2}	55.05 μH	Inductance of R_{X2}	55.43 μH
Capacitance of T_{X2}	287 nF	Capacitance of R_{X2}	285 nF
Core material of WPT		Ferrite	
Core material of matching inductor		SENDUST	

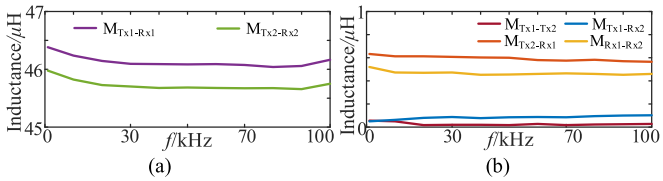

Fig. 7. Measured inductance of the coupling structure. (a) Coupled inductance among targeted coils. (b) Coupled inductance among untargeted coils.

D. System Control

To ensure WUM normal operation, two channels of high-frequency balanced voltage with 90° phase angle difference should be provided for the two-phase of the ultrasonic motor. Meanwhile, the two channels of high-frequency voltage should be adjustable in voltage, frequency, and phase position by transmitting side controller.

Fig. 5 shows the motor control method of the WUM, which is implemented by two modes, including low-speed mode and high-speed mode. In the low-speed zone, the motor speed is controlled by frequency, while in high-speed zone, it is controlled by voltage amplitude. The direction is controlled by the phase difference of u_{AZ} and u_{BZ}.

The reason of two modes control is that there is low-speed dead zone in voltage-speed control mode due to the characteristic of the WUM. The frequency-speed method can reach to

TABLE II
COMPARISON WITH OTHER WIRELESS DRIVES

Ref.	Motor type	Resonant frequency	Compensation network	Bidirectional power flow	No. Rx side diodes	No. Rx side Mos	No. Tx tanks	Transmission efficiency*
[8]	IM	90.47,130.64 kHz	LC-LCLCC	No	8	8	1	83.5%
[10]	DCM	130,160 kHz	LCL-LC	No	10	2	1	85%
[11]	SRM	90,110,130 kHz	LCCL-LC	No	12	0	1	80%
[12]	SRM	100 kHz	LC-LC	No	12	0	3	89.1%
[13]	IM	109,116 kHz	LCL-Cap banks	No	4	4	1	86.2%
Proposed	UM	40 kHz	LC-LC	No	0	0	2	86.6%–92%

Notes: IM: induction motor, SRM: switched reluctance motor, DCM: direct current motor, UM: ultrasonic motor. *: not power to load efficiency.

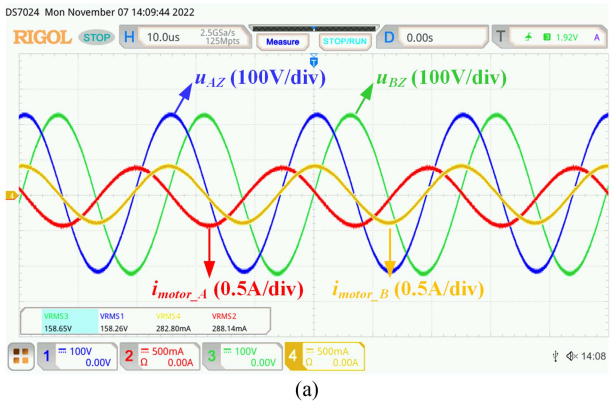

Fig. 8. Experimental performance. (a) Measured voltage and current of wireless ultrasonic motor. (b) Measured voltage and current of transmitting side and wireless motor under 2 mH matching inductors.

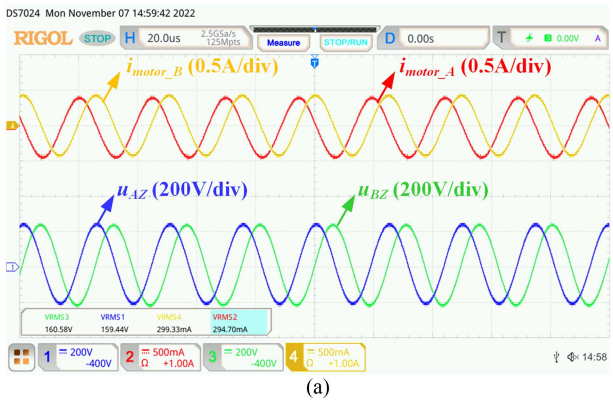

Fig. 9. Experimental performance of voltage and current of wireless ultrasonic motor at 4.8 and 12.6 r/min.

lower speed when control frequency is smaller than the resonant frequency. However, the linearity of frequency-speed decreases sharply when the control frequency is larger than the resonant frequency. Thus, when the control frequency rises up to the resonant frequency, the motor speed is controlled by adjusting voltage amplitude, which is usually implemented by adjust duty cycle in controller. Besides, the closed-loop speed or position control is implemented with the help of the encoder information transferred with the Bluetooth [10], [11], [12], [13].

III. EXPERIMENTAL ANALYSIS

A. Experimental Setup

In order to validate the proposed WUM drive, an experimental prototype is built and shown in Fig. 6 in which the voltage and current are measured by probes Rigol RP1050D and Tektronix TCP300, respectively, and displaced in the oscilloscope Rigol DS7000. The MOSFETs of the inverter is from CREE C3M0065090D. The gate driver is from TI UCC21521. Under voltage lock out, programmable dead time, current protection, and output PWM voltage protection are adopted for the driver circuit to avoid failure. The control algorithm is implemented in the DSP TMS320F28335 from TI. The encoder output is shown in oscilloscope by using a digital to analog module for precisely observation of the motor rotational status. The key experimental parameters are listed in Table I.

B. Experimental Performance

First, the coupled inductance of the transmitting coils and receiving coils are tested to verify the transmitting ability of the coupling structure. The coupled inductances are demonstrated

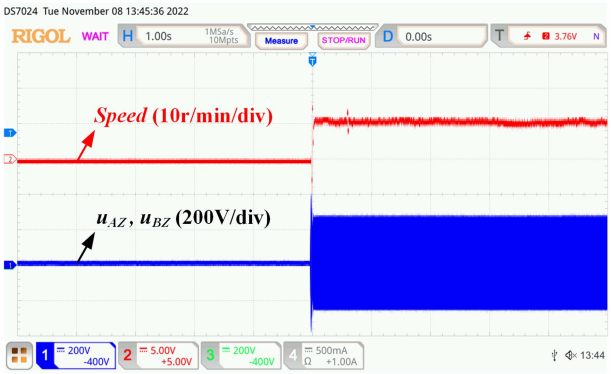

(a)

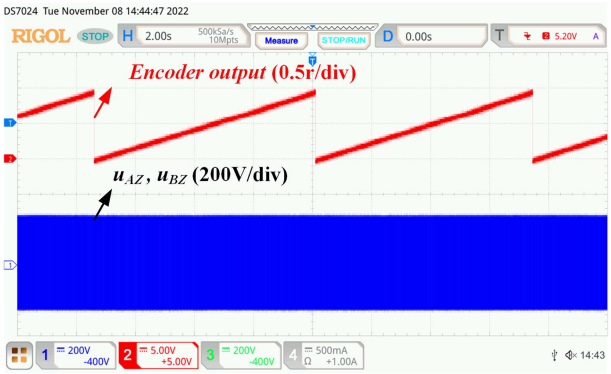

(b)

Fig. 10. Measured motor speed and motor voltage. (a) Startup performance from 0 to 10 r/min. (b) Experimental performance of encoder output and voltage of wireless motor at 8.7 r/min.

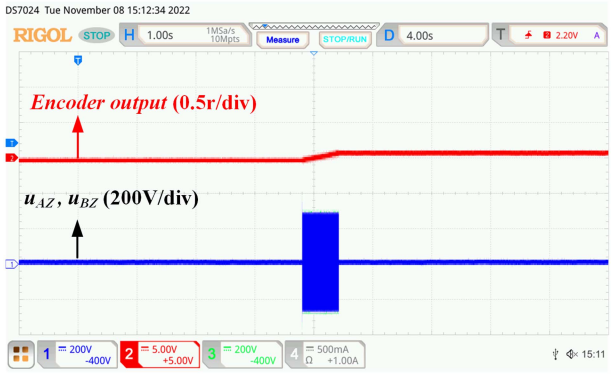

(a)

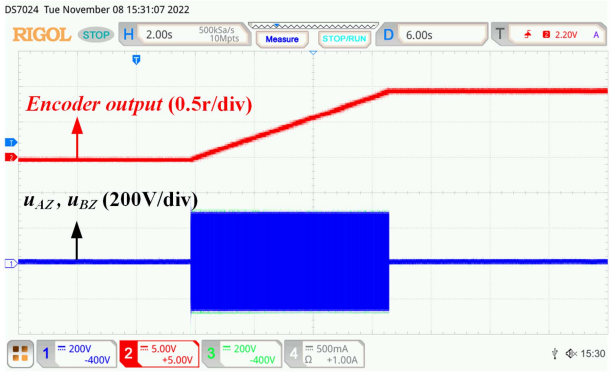

(b)

Fig. 11. Experimental performance of encoder output and voltage of wireless ultrasonic motor rotating to specific angles. (a) 36° mechanical angle. (b) 360° mechanical angle.

in Fig. 7. It can be seen that the coupled inductances among untargeted coils are near zero, while it is about 46 μH between the targeted coils.

Second, the performances of the WUM drive system are tested. The measured two-phase voltages and currents of wireless motor are demonstrated in Fig. 8(a). The amplitude of the two-phase voltages and currents are 158.65 and 158.26 V, 282.80 and 288.14 mA, respectively, which shows the two-phase voltages and currents are well balanced. The phase angle of the two-phase motor voltages and currents are 90°. Moreover, they are sinusoidal, which agrees the drive requirements of the WUM.

Third, the function of the matching circuit is presented in Fig. 8(b). The transmitting voltage u_{Tx1} is in the same phase with the transmitting current i_{Tx1}, which shows the total reflecting impendence of the receiving side is resistive. Thus, the 2 mH matching inductor realizes the goal of filtering harmonic voltages and impedance matching. It also needs to mention that the wireless motor may not start up if the matching inductance deviates from the calculated value too much.

Fourth, the performance of the two-phase motor voltage and current under different rotational speed are demonstrated in Fig. 9, including 4.8 and 12.6 r/min. It is observed that the speed increases, the motor voltage and current reach higher.

Fifth, the startup performance from 0 to 10 r/min is shown in Fig. 10(a), including the speed and two-phase motor voltage.

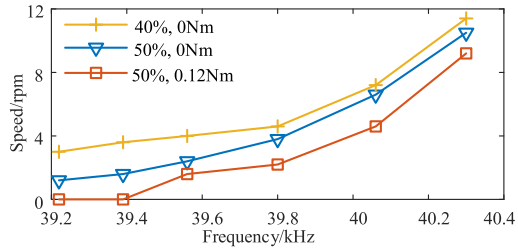

Fig. 12. Speed control with different control frequencies.

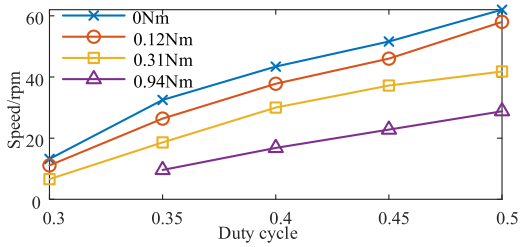

Fig. 13. Speed control for different loads with duty cycles.

The motor can start up within one speed sample period 5 ms, which shows quick response of the wireless motor. Fig. 10(b) shows the encoder output and two-phase motor voltage of the wireless motor, which shows the WUM rotates smoothly.

It needs to mention that the propagation delay of the Bluetooth will influence the dynamic performance of the motor control. In the proposed wireless drive, the propagation delay is less than the update of the speed loop, which has very limited influence on the motor control, especially position control. If good dynamic performance is required, other methods should be considered, such as electromagnetic type communication.

Finally, wireless motor usually needs to rotate to a scheduled angle to complete specified action. Thus, the performance of rotating with a specific angle is tested in Fig. 11, including 36° and 360°. It is observed that the WUM can rotate to the scheduled angles in good response. Meanwhile, the rotating period is freely adjusted by the motor speed.

Fig. 12 demonstrates the performance of the low-speed zone with different control frequencies, which can realize accurate speed control from 0 to 10 rpm. Fig. 13 shows the speed-duty cycle control performance for different loads in high-speed zone. It is observed that when the duty cycle is lower than 0.3, the wireless drive cannot start up. Besides, the minimum speed with duty cycle control is far more than the speed with frequency control, which shows that frequency control can extend the low-speed zone of the wireless motor and prove effectiveness of the two speed zone control strategy.

A comparison is made with other wireless drives, as shown in Table II. It needs to be clear that only transmission efficiency rather than dc source to load efficiency is provided in other wireless drive literatures, so only transmission efficiency is listed for a fair comparison. The transmission efficiency is a bit higher than other wireless drive, because of fewer MOSFETs used at the transmitting side and no diode used at the receiving side.

IV. Conclusion

In this letter, a new WUM system is proposed. The proposed system guarantees that no controller or active device exists at the transmitting side. Besides, regular maintenance and output ripple resulted from other wireless motor are avoided by using the proposed WUM. The design procedures, operating principles, and motor control method are demonstrated in detail. The experimental results with the steady-state and transient performances verify the feasibility and correctness of the WUM drive system.

References

[1] Z. Zhang, H. Pang, A. Georgiadis, and C. Cecati, "Wireless power transfer—An overview," *IEEE Trans. Ind. Electron.*, vol. 66, no. 2, pp. 1044–1058, Feb. 2019.

[2] Y. Xiao and C. Liu, "Direct load voltage control for electrolytic capacitor-less wireless power transfer system without DC/DC converter," *IEEE Trans. Ind. Electron.*, vol. 68, no. 9, pp. 8039–8048, Sep. 2021.

[3] Y. Li, J. Hu, X. Li, H. Wang, and K. W. E. Cheng, "Cost-effective and compact multistring LED driver based on a three-coil wireless power transfer system," *IEEE Trans. Power Electron.*, vol. 34, no. 8, pp. 7156–7160, Aug. 2019.

[4] W. Han, K. T. Chau, and Z. Zhang, "Flexible induction heating using magnetic resonant coupling," *IEEE Trans. Ind. Electron.*, vol. 64, no. 3, pp. 1982–1992, Mar. 2017.

[5] A. Babaki, S. Vaez-Zadeh, M. Jahanpour-Dehkordi, and A. Zakerian, "Wireless motor drives with a single inverter in primary side of power transfer systems," in *Proc. IEEE PELS Workshop Emerg. Technol.: Wireless Power Transfer*, 2019, pp. 125–128.

[6] Z. Yan, B. Song, Y. Zhang, K. Zhang, Z. Mao, and Y. Hu, "A rotation-free wireless power transfer system with stable output power and efficiency for autonomous underwater vehicles," *IEEE Trans. Power Electron.*, vol. 34, no. 5, pp. 4005–4008, May 2019.

[7] K. Song et al., "A rotation-lightweight wireless power transfer for solar wing driving," *IEEE Trans. Power Electron.*, vol. 34, no. 9, pp. 8816–8830, Sep. 2019.

[8] W. Liu, K. T. Chau, C. H. T. Lee, L. Cao, and W. Han, "Wireless power and drive transfer for piping network," *IEEE Trans. Ind. Electron.*, vol. 69, no. 3, pp. 2345–2356, Mar. 2022.

[9] A. Abdolkhani, A. P. Hu, and N. -K. C. Nair, "A double stator through-hole type contactless slipring for rotary wireless power transfer," *IEEE Trans. Energy Convers.*, vol. 29, no. 2, pp. 426–434, Jun. 2014.

[10] C. Jiang, K. T. Chau, C. H. T. Lee, W. Han, W. Liu, and W. H. Lam, "A wireless servo motor drive with bidirectional motion capability," *IEEE Trans. Power Electron.*, vol. 34, no. 12, pp. 12001–12010, Dec. 2019.

[11] C. Jiang, K. T. Chau, W. Liu, C. Liu, W. Han, and W. H. Lam, "An LCC-compensated multiple-frequency wireless motor system," *IEEE Trans. Ind. Inform.*, vol. 15, no. 11, pp. 6023–6034, Nov. 2019.

[12] W. Han, K. T. Chau, Z. Hua, and H. Pang, "An integrated wireless motor system using laminated magnetic coupler and commutative-resonant control," *IEEE Trans. Ind. Electron.*, vol. 69, no. 5, pp. 4342–4352, May 2022.

[13] H. Wang, K. T. Chau, C. H. T. Lee, L. Cao, and W. H. Lam, "Design, analysis, and implementation of wireless shaded-pole induction motors," *IEEE Trans. Ind. Electron.*, vol. 68, no. 8, pp. 6493–6503, Aug. 2021.

[14] M. Kühne, R. G. Rochín, R. S. Cos, G. J. R. Astorga, and A. Peer, "Modeling and two-input sliding mode control of rotary traveling wave ultrasonic motors," *IEEE Trans. Ind. Electron.*, vol. 65, no. 9, pp. 7149–7159, Sep. 2018.

[15] J. Wu, Y. Mizuno, and K. Nakamura, "A rotary ultrasonic motor operating in torsional/bending modes with high torque density and high power density," *IEEE Trans. Ind. Electron.*, vol. 68, no. 7, pp. 6109–6120, Jul. 2021.

[16] J. Shi and B. Liu, "Optimum efficiency control of traveling-wave ultrasonic motor system," *IEEE Trans. Ind. Electron.*, vol. 58, no. 10, pp. 4822–4829, Oct. 2011.

[17] X. Li, J. Hu, Y. Li, H. Wang, M. Liu, and P. Deng, "A decoupled power and data-parallel transmission method with four-quadrant misalignment tolerance for wireless power transfer systems," *IEEE Trans. Power Electron.*, vol. 34, no. 12, pp. 11531–11535, Dec. 2019.